Supporting information

Highly intensive red luminescent benzotriazolate complex of $\{Mo_6I_8\}$ with {Ag(*t*BuXPhos)}

Elena Gorbachuk,*[a,b] Maxim Mikhaylov,[c] Kirill Tagiltsev,[c] Vasily Yudin,[c] Taisiya Sukhikh,[c] Aleksandr Sukhov,[a,b] Bulat Faizullin,[a] Artemiy Shmelev,[d] Viktor Nikiforov,[d] Maxim Sokolov[c] and Dmitry Yakhvarov*[a,b]

[a] Arbuzov Institute of Organic and Physical Chemistry, FRC Kazan Scientific Center, Russian Academy of Sciences, Arbuzov str., 8, 420088 Kazan (Russian Federation).
[b] Alexander Butlerov Institute of Chemistry, Kazan Federal University, Kremlyovskaya str., 18, 420008 Kazan (Russian Federation).
[c] Nikolaev Institute of Inorganic Chemistry SB RAS, Acad. Lavrentiev Ave., 3, 630090 Novosibirsk (Russian Federation).
[d] Zavoisky Physical-Technical Institute, FRC Kazan Scientific Center of RAS, 10/7 Sibirskiy trakt, 420029 Kazan (Russian Federation).

Materials and Characterization

Materials, *t*BuXPhos, HOTf (OTf = SO_3CF_3), Sodium tetraphenylborate $NaBPh_4$, 1-trimethylsilyl-1,2,3-benzotriazole (TMSBTA), benzotriazole (HBTA), acetone, acetonitrile, dichloromethane, diethyl ether, ethanol were obtained from commercial suppliers (e.g., Sigma-Aldrich, Alfa Aesar, TCI, Fisher Scientific) and used without additional purification. $(TBA)_2[Mo_6I_8(OAc)_6]$ (where OAc = acetate) was obtained according to the published method.[1] AgOTf and AgOAc were obtained by the reactions of TfOH and Ag_2O,[2] HOAc with Ag_2CO_3,[3] respectively.

Methods

IR spectra were recorded on SCIMITAR FTS 2000 (4000–400 cm^{-1}) and VERTEX 80 (600–100 cm−1) Fourier spectrometers.

Energy-dispersive X-ray analysis (EDX) was carried out on a Hitachi Tabletop Microscope TM-3000 equipped with EDS System QUANTAX 70.

Thermogravimetric analysis was performed on a NETZSCH STA 449 F1 Jupiter thermal analyzer. The measurements were made in a helium-hydrogen mixture (10.0 vol.% H2) in the temperature range of 30–600°C, flow rate 30 ml/min, open Al_2O_3 crucible, heating rate of 10 °C/min. The experimental results were processed using a standard Proteus Analysis software (NETZSCH Proteus Thermal Analysis v.6.1.0 (2013). NETZSCH-Gerätebau GmbH, Selb/Bayern, Germany).

^1H NMR and ^{13}C NMR spectra were recorded on a 500 MHz NMR spectrometer, Bruker Avance 500 plus.

Mass spectrometry data were obtained on a liquid chromatograph — mass spectrometer (LC-MC) from Agilent (6130 Quadrupole MS, 1260 infinity LC). The analysis was performed in the mass range of 350–3000 amu for both positively and negatively charged ions in SCAN mode. Electrospray ionization was used as the ionization source. A flow of nitrogen gas, temperature 350°C, flow rate 7 L/min; pressure at the atomizer (nitrogen) 60 psig; and voltage at the capillary

4000 V served as the desiccant. In order to preserve weakly bound forms in the mass spectra, the voltage across the fragmenter was zero in all experiments. A solution of the tested compound (5 μL) in deuterated acetonitrile with a concentration of ~10^{-4} g/mL was injected into the mobile phase (acetonitrile "h.p.") at a flow rate of 0.4 mL/min, atomized, and ionized. Experimental peaks were compared with calculated peaks, including isotopic distribution. The Molecular Weight Calculator by Matthew Monroe program was used for the calculations.

Elemental analysis was performed at the Analytical Laboratory of IIC SB RAS on a Euro EA 3000 CHNS analyzer.

Single crystal X-ray diffraction (SXRD). Single-crystal XRD data were collected at 150 K with a Bruker D8 Venture diffractometer equipped with a CMOS PHOTON III detector and IμS 3.0 microfocus source (MoKα radiation (λ = 0.71073 Å) or CuKα radiation (λ = 1.54178 Å), collimating Montel mirrors). Data reduction was performed routinely via the APEX 3 suite. The crystal structures were solved using the ShelXT[4] and refined using ShelXL[5] programs assisted by Olex2 GUI[6]. Hydrogen atoms were placed geometrically. Atomic displacements for non-hydrogen atoms were refined in harmonic anisotropic approximation with the exception for disordered solvate molecules.

Structure **1** reveals a disorder of co-crystallized benzotriazole over two positions; its geometry was refined with appropriate restraints.

Structure **2** reveals a disorder of benzotriazolate, and severe disorder of Na cations and water sharing proximate positions. Free refinement of the sum occupancy of Na in two disordered positions Na1A and Na1B gives the value of 0.6, which is in line with EDX analysis, supporting an overall Na:Mo ratio of 1.6:6. Charge balance is maintained by H^+, likely as H_3O^+ or protonated ligand. Therefore, residual density in the solvent regions is highly diffuse and involves a complex mixture of Na^+, H_2O and H_3O^+ distributed over numerous partially occupied sites. However, resolving this disorder would require extensive quantum chemical calculations to distinguish between competing disorder models, which is beyond the scope of this work. However, the location and precise arrangement of solvent molecules does not affect the key structural moments discussed.

The structure of **4** was of insufficient quality due to somewhat low diffraction intensity and unresolvable disorder of one of {*t*BuXPhos-Ag} fragment and triflates. Only main structural features, i.e. the Mo_6I_8 cluster geometry, the connectivity of benzotriazolate ligands, the presence of coordinated Ag, and the overall architecture, were determined. These features coincide with those found for the analogous structure of **4b**. The structure was submitted to the Cambridge Structural Database (CSD) as a CSD Communication (deposition number 2491982). The unit cell parameters for structure **4** are: *P*–1, a = 17.6045(9), b = 17.9300(13), c = 24.0454(12), α = 74.337(5)°, β = 83.325(4)°, γ = 60.819(3)°, V = 6379.5(7) Å^3.

Structures **2** and **4b** reveal severe disorder of some solvate molecules and triflate anions that were not modelled explicitly, but their contribution was treated via Solvent Mask Procedure in Olex2. In structure **2**, 1095 electrons were found in a volume of 2062 Å^3 in one void per unit cell, ascribed to 6 H_2O and 4 C_2H_6O per formula unit. In structure **4b**, 276 electrons were found in a volume of 1206 Å^3 in one void per unit cell, ascribed to 10 C_2H_6O per formula unit. In **4b**, the disordered triflate anions were modelled explicitly in rigid body approximation. The disorder model including geometrically feasible combinations of occupied triflate positions is shown in Fig. S25 and briefly discussed in the caption to the figure.

The structures were deposited to the Cambridge Crystallographic Data Centre (CCDC) as a supplementary publication, No. 2491979-2491981, 2491983, and 2491984.

Powder X-ray diffraction (PXRD). Powder XRD data were collected with the same diffractometer (λ = 1.54178 Å) at 150 K. Samples were prepared by grinding of the powders and put into a glass capillary. By φ-scanning (360°), Debye diffraction patterns with continuous diffraction arcs were measured.[7,8]. To diminish the effect of the preferred orientations, five scans were made at different positions of a goniometer for ω from –240° to 0°. The external standard (Si) correction and integration were performed using the Dioptas 0.5.4 program.[9]

The HORIBA Fluorolog QM-75-22-C spectrofluorometer was used to investigate luminescence parameters. The recording channel was equipped with a double grating monochromator (380 nm focal length, 1200 grooves/mm, blaze 500 nm) and a TEM-cooled Hamamatsu R13456-11 photomultiplier tube. A 75 W Xenon lamp was used as an excitation source, passing through the double grating (1200 groove/mm, 500 nm blaze, focal length 380 nm). The sample powder was cooled using a Janis ST-100 cold finger cryostat installed into the sample chamber with a Lake Shore 325 temperature controller. The temperature accuracy was better than 0.1 K, and cooling was achieved using liquid nitrogen. The quantum yield of the samples was measured at room temperature using a Horiba petite integration sphere mounted in the sample compartment. Time-correlated single-photon counting (TCSPC) was used for lifetime measurements. A DD405L nanosecond laser with a pulse duration of 5 nanoseconds (FWHM) was used as an excitation source. Luminescence was recorded using an R13456-11 PMT in photon-counting mode. The time-to-digital converter and laser were synchronized using DeltaHub controller. The resulting kinetics of luminescence were fitted using an optimal two-exponential decay model. The fit is reliable for relative intensities above 10^{-5}, which covers the relevant dynamic range in all cases studied. The first 35 nanoseconds were excluded from the analysis using the instrument response function (IRF).

Synthesis of 1.

The cluster salt $(TBA)_2[Mo_6I_8(OAc)_6]$ (500 mg, 0.205 mmol) was added to 3 mL of TMSBTA (3.21 g, 16.8 mmol). The reaction mixture was degassed and kept at 100°C for two days. After heating, acetone was added to the solution, which was then filtered through a paper filter. Diethyl ether was added to the filtrate, and the resulting suspension was placed in a freezer overnight to ensure complete precipitation. The formed beige precipitate was filtered through a glass filter (G4), washed with diethyl ether, and dried under an air stream. Yield: 454 mg (68%). Elemental analysis: calcd (%) for $(TBA)_2[Mo_6I_8(BTA)_6]\cdot 4HBTA$, $C_{92}H_{116}N_{32}Mo_6I_8$ (3271.7) C: 33.7%, H: 3.6%, N: 13.7%; found: C: 33.4%, H: 3.7%, N: 13.5%. MS (ESI-MS) *m/z* (%): calc. 1150.5, found 1150.5 (for $[Mo_6I_8(BTA)_6]^{2-}$), calc. 2542.2, found 2542.2 (for $(TBA)[Mo_6I_8(BTA)_6])^-$). Single crystals of $(TBA)_2[Mo_6I_8(BTA)_6]\cdot 4HBTA$, suitable for X-ray diffraction analysis, were obtained by slow vapor diffusion of diethyl ether into an acetone solution of the reaction mixture. ^{1}H NMR (CD_3CN; δ (for BTA-ligands), ppm): 7.89 (d, 12 H, ^{3}J = 5.0 Hz, H-C(4), H-C(7)), 7.70 (t, 12 H, ^{3}J = 5 Hz, H-C(5), H-C(6)), 7.61 (d, 12 H, ^{3}J = 5.0 Hz, H-C(4), H-C(7)), 7.28 (t, 12 H, ^{3}J = 5 Hz, H-C(5), H-C(6)), 7.16 (t, 12 H, ^{3}J = 5 Hz, H-C(5), H-C(6)). IR spectrum (KBr), ν (cm^{-1}): 2960 ÷ 2916 (broad, s), 1647 (m), 1620 (m), 1604 (m), 1573 (w), 1477 (m), 1460 (w), 1442 (m), 1388 (w), 1381 (w), 1361 (w), 1304 (w), 1271 (m), 1256 (m), 1207 (m), 1165 (w), 1146 (w), 1126 (w), 1109 (w), 1047 (s), 1008 (w), 986 (m), 908 (w), 877 (m), 846 (w), 775 (m), 746 (s), 682 (w), 634 (w), 576 (w), 545 (w), 438 (w). Far-IR (polyethylene), ν (cm^{-1}): 545 (s), 437 (s), 316 (m), 304 (m), 278 (w), 218 (s), 151 (s), 120 (m).

Table S1. Crystal data and structure refinement for the compounds.

Identification code	**1**	**2**	**3**	**3b**	**4b**
Empirical formula	$C_{92}H_{116}I_8Mo_6N_{32}$	$C_{44}H_{67.4}I_8Mo_6N_{18}Na_{1.6}O_{13.5}$	$C_{32}H_{48}AgF_3NO_3PS$	$C_{60}H_{90}Ag_2F_6O_6P_2S_2$	$C_{235}H_{357}Ag_6F_{12}I_8Mo_6N_{18}O_{22.5}P_6S_4$
Formula weight	3261.00	2692.18	722.61	1363.11	6574.48
Temperature/K	150(2)	150(2)	150(2)	150(2)	150(2)
Space group	*P*–1	*P*2/*c*	$P2_1/c$	$P2_1/n$	*P*–1
a/Å	12.4843(2)	18.6854(4)	9.0695(11)	10.9171(2)	17.8066(10)
b/Å	12.7328(2)	14.5791(3)	22.929(2)	20.4854(3)	19.1013(10)
c/Å	17.9457(4)	26.4243(5)	16.5120(17)	14.6193(3)	22.6846(13)
α/°	107.1970(10)	90	90	90	111.715(4)
β/°	91.0880(10)	101.1580(10)	100.459(4)	103.6375(5)	100.983(4)
γ/°	100.8710(10)	90	90	90	98.710(4)
Volume/Å^3	2667.71(9)	7062.3(2)	3376.6(6)	3177.30(10)	6825.4(7)
Z	1	4	4	2	1
ρ_{calc}g/cm^3	2.030	2.551	1.421	1.425	1.600
μ/mm^{-1}	3.059	4.609	0.755	0.797	13.814
F(000)	1568.0	5116.0	1504.0	1416.0	3293.0
Crystal size/mm^3	0.16 × 0.07 × 0.05	0.16 × 0.05 × 0.03	0.26 × 0.06 × 0.04	0.11 × 0.1 × 0.08	0.09 × 0.04 × 0.025
Radiation	MoKα (λ = 0.71073)	MoKα (λ = 0.71073)	MoKα (λ = 0.71073)	MoKα (λ = 0.71073)	CuKα (λ = 1.54178)
2Θ range for data collection/°	4.262 to 55.832	4.922 to 51.364	3.074 to 58.26	3.976 to 59.16	4.352 to 149.678
Index ranges	$-16 \le h \le 16$, $-16 \le k \le 16$, $-23 \le l \le 23$	$-22 \le h \le 22$, $-17 \le k \le 17$, $-32 \le l \le 32$	$-12 \le h \le 12$, $-31 \le k \le 28$, $-21 \le l \le 22$	$-15 \le h \le 15$, $-18 \le k \le 28$, $-19 \le l \le 18$	$-22 \le h \le 22$, $-23 \le k \le 23$, $-28 \le l \le 28$
Reflections collected	50625	67737	44550	23275	88250
Independent reflections	12747 [R_{int} = 0.0324, R_{sigma} = 0.0288]	13389 [R_{int} = 0.0633, R_{sigma} = 0.0487]	9023 [R_{int} = 0.0694, R_{sigma} = 0.0621]	8702 [R_{int} = 0.0397, R_{sigma} = 0.0474]	27385 [R_{int} = 0.1163, R_{sigma} = 0.1072]
Restraints/parameters	99/654	228/677	0/392	28/381	1109/1551
Goodness-of-fit on F^2	1.035	1.049	1.055	1.036	0.950
Final R indexes [I>=2σ (I)]	R_1 = 0.0240, wR_2 = 0.0523	R_1 = 0.0423, wR_2 = 0.1129	R_1 = 0.0521, wR_2 = 0.1178	R_1 = 0.0348, wR_2 = 0.0707	R_1 = 0.0536, wR_2 = 0.1222
Final R indexes [all data]	R_1 = 0.0300, wR_2 = 0.0562	R_1 = 0.0597, wR_2 = 0.1244	R_1 = 0.0702, wR_2 = 0.1269	R_1 = 0.0461, wR_2 = 0.0776	R_1 = 0.0949, wR_2 = 0.1414
Largest diff. peak/hole / e Å^{-3}	0.86/-0.73	1.74/-1.02	0.71/-0.83	0.60/-0.32	1.22/-0.96

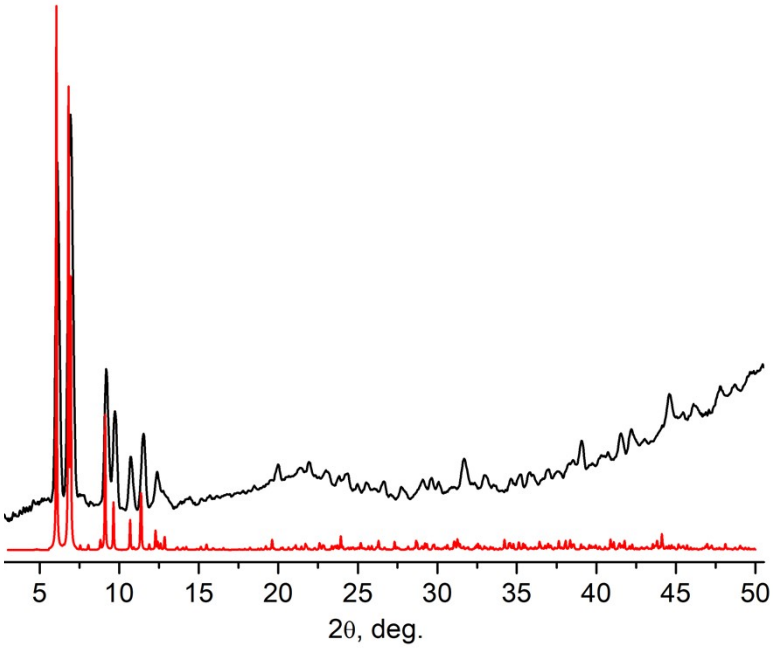

Fig. S1. Experimental (black) and simulated (red) powder XRD patterns of **2**.

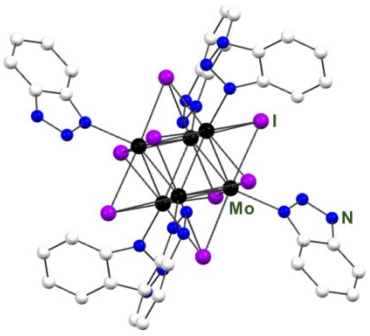

Fig. S2. Crystal structure of anion $[Mo_6I_8(BTA)_6]^{2-}$ **1**.

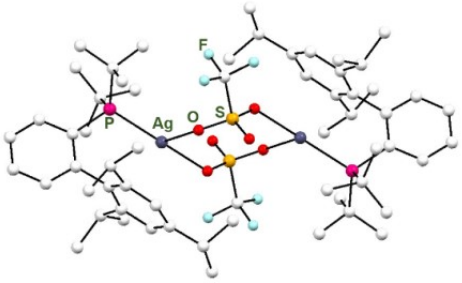

Fig. S3. Crystal structure of **3b**.

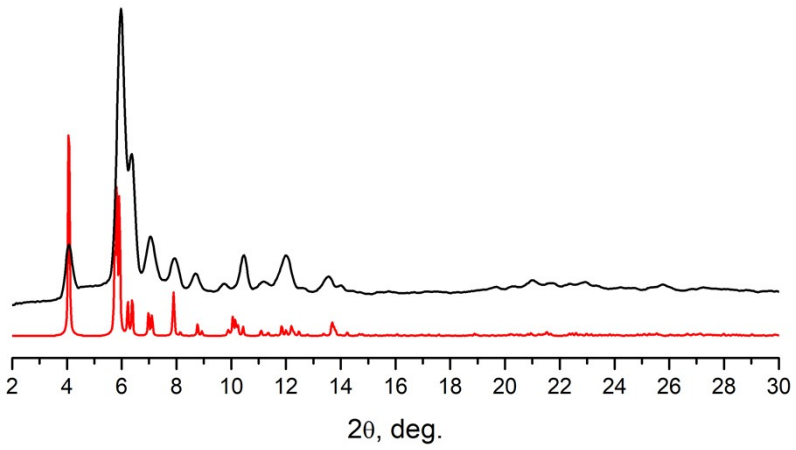

Fig. S4. Experimental (black) and simulated (red) powder XRD patterns of **4**.

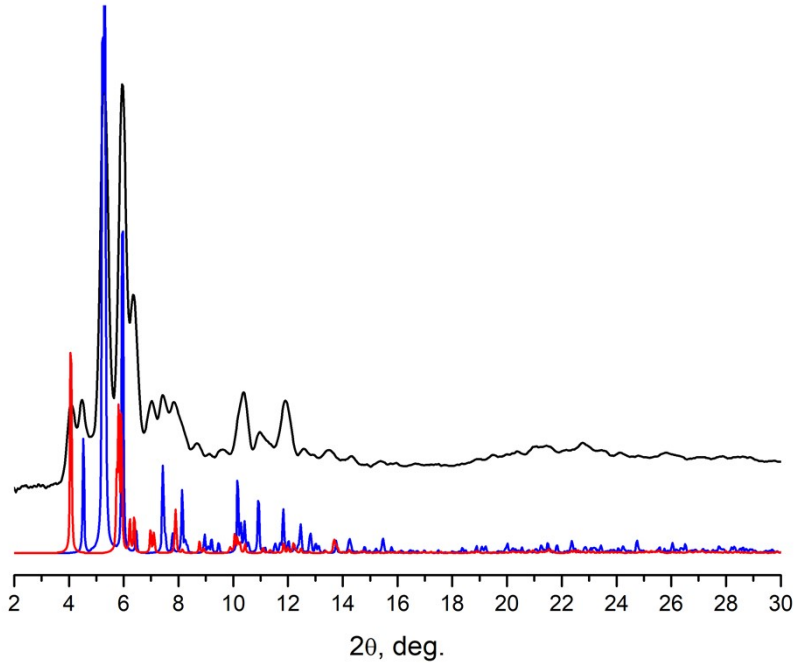

Fig. S5. Experimental powder XRD pattern for the mixture of phases **4** and **4b** (black) and simulated for **4** (red) and for **4b** (blue) patterns.

Table S2. Ag…C and Ag…π distances (Å) in the complexes. C_6 plane designates the mean plane formed by six C atoms of the phenyl fragment closest to Ag, C_6 centroid designates the corresponding centroid.

	Ag…C_{ipso}	Ag…C_{ortho}	Ag…(C_6 plane)	Ag…(C_6 centroid)
4b	2.930(11), 2.690(8), 2.874(13)	2.825(9), 2.835(6), 3.009(7)	2.676(6), 2.763(7), 2.813(4)	2.958(5), 3.054(5), 3.089(3)
3b	2.960(2)	3.012(2)	2.8968(13)	3.0453(10)
3	3.020(3)	2.910(3)	2.866(2)	3.1172(13)

Table S3. Summary of the examples of highly intensive red-emitting ($\Phi_L > 0.60$) $\{Mo_6I_8\}L_6$ cluster structures and in this work.

L	$\tau_{em(\mu s)}$	λ_{em} (nm)	Φ_L	Conditions
	$NBu_4\{Mo_6I_8\}L_6$			
CF_3COO	333;[1] 182[10]	668;[1] 693[10]	0.67;[1] 1[10]	acetonitrile
C_2F_5COO	353[1]	668[1]	0.73[1]	acetonitrile
C_3F_7COO	359[1]	668[1]	0.6[1]	acetonitrile
	340[11]	675[11]	0.64[11]	acetone
Ph–COO	299[1]	702[1]	0.62[1]	acetonitrile
pyrene–COO	210[12]	698[12]	0.6[12]	THF
$C_{10}H_{15}COO$ $C_{10}H_{15}$ = adamantane	225[13]	710[13]	0.76[13]	THF
4`-carboxybenzo-15-crown-5	231[14]	710[14]	0.71[14]	DMSO
cholate	221[11]	705[11]	0.64[11]	DMSO
OTs = *p*-toluenesulfonate	305[15]	667[15]	0.65[15]	acetonitrile
1-OOC-1,12-closo-$C_2B_{10}H_{11}$	330[16]	685[16]	0.77[16]	acetonitrile
1-OOC-1,7-closo-$C_2B_{10}H_{11}$	320[13]	685[13]	0.93[13]	acetonitrile
1-OOC-1,2-closo-$C_2B_{10}H_{11}$	360[13]	685[13]	0.7[13]	acetonitrile
$PhSO_3$ = benzenesulfonate	263[17]	665[17]	0.6[17]	acetonitrile
$PhSO_3$	τ_1 = 183 (0.60), τ_2 = 57 (0.40)[17]	657[17]	0.62[17]	solid state
$Kat_2[\{Mo_6I_8\}L_6$ (Kat = trialkylmethylammonium cation bearing cyanobiphenyl-terminated decyloxy chains)				
CF_3COO[18]	τ1 = 48 (0.60)[18] τ2 = 4.8 (0.40)	ca. 660[18]	0.70[18]	solid state (in air)
C_2F_5COO	τ1 = 50 (0.72) [18] τ2 = 5.0 (0.28)	ca. 660[18]	0.70[18]	solid state (in air)
C_3F_7COO	τ1 = 51 (0.66) [18] τ2 = 5.0 (0.34)	ca. 660[18]	0.70[18]	solid state (in air)
$Na_2\{Mo_6I_8\}L_6$				
2-[2-(2-methoxyethoxy)ethoxy] acetate	232[19]	700[19]	0.71 ± 0.09[19]	DMSO
$Na_{2-x}\{H\}_x[\{Mo_6I_8\}L_6]$ **2**				
BTA = benzotriazolate (this work) **2**	τ_1 = 40.5 τ_2 = 83.3	702	0.43	solid state (deaerated), 300 K
	τ1 = 106.7 τ2 = 171.8	738		solid state (deaerated), 77 K
$[\{Mo_6I_8\}L_6]OTf_4$				
*t*BuXPhosAg(BTA) (this work) **4**	τ_1 = 81.1 τ_2 = 161.1	675	> 0.96	solid state (deaerated), 300 K
	τ_1 = 170.7 τ_2 = 355.4	640		solid state (deaerated), 77 K

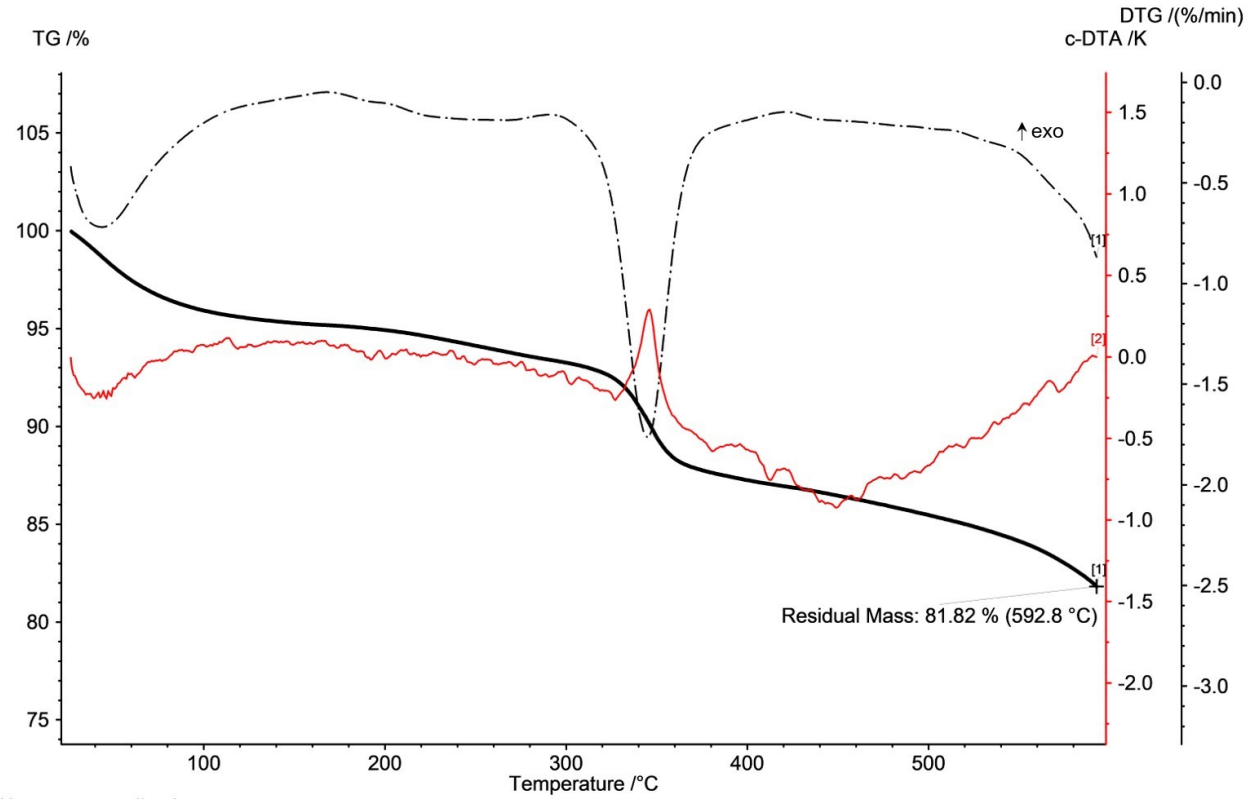

Figure S6. Data from the thermogravimetric analysis of **2**.

NMR Spectra

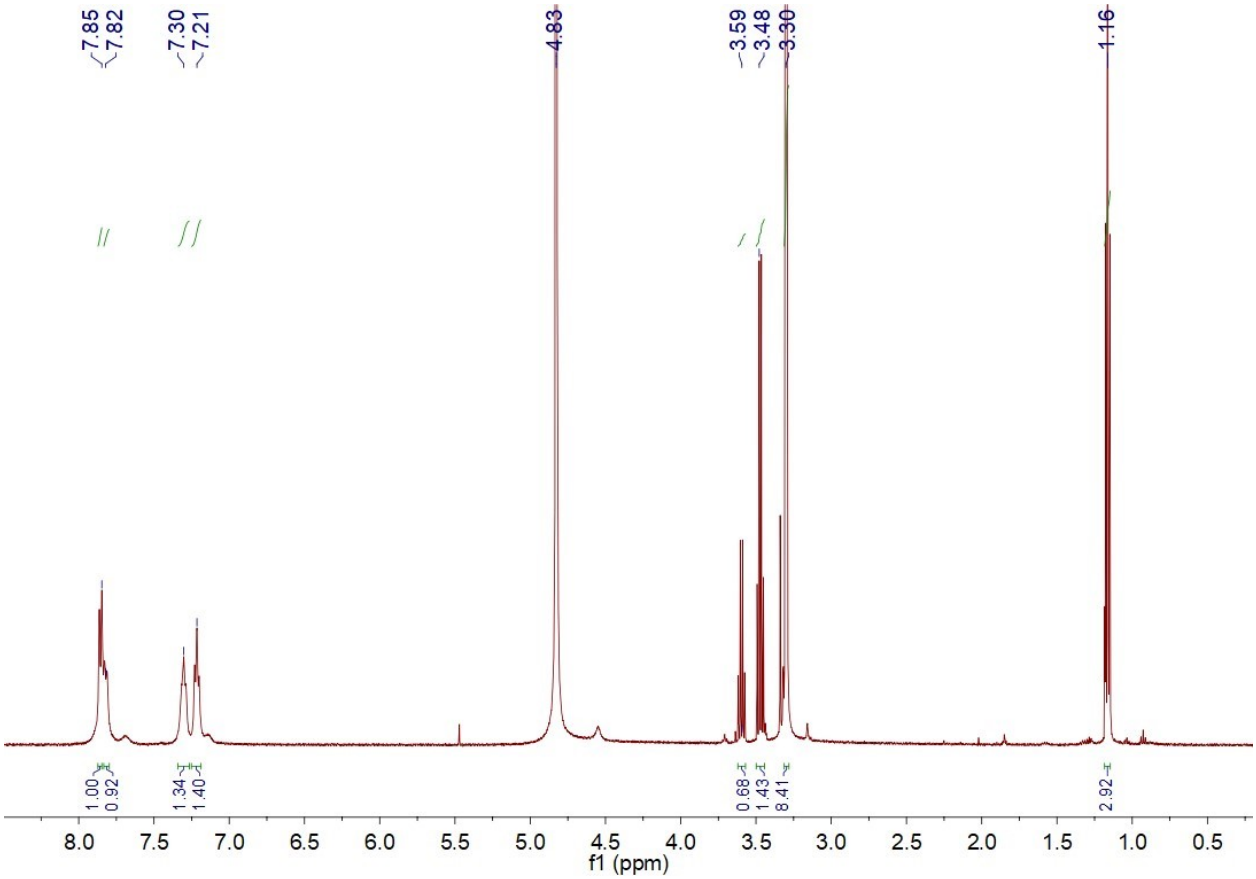

Figure S7. ^{1}H NMR spectrum of **2** (CD_3OD)

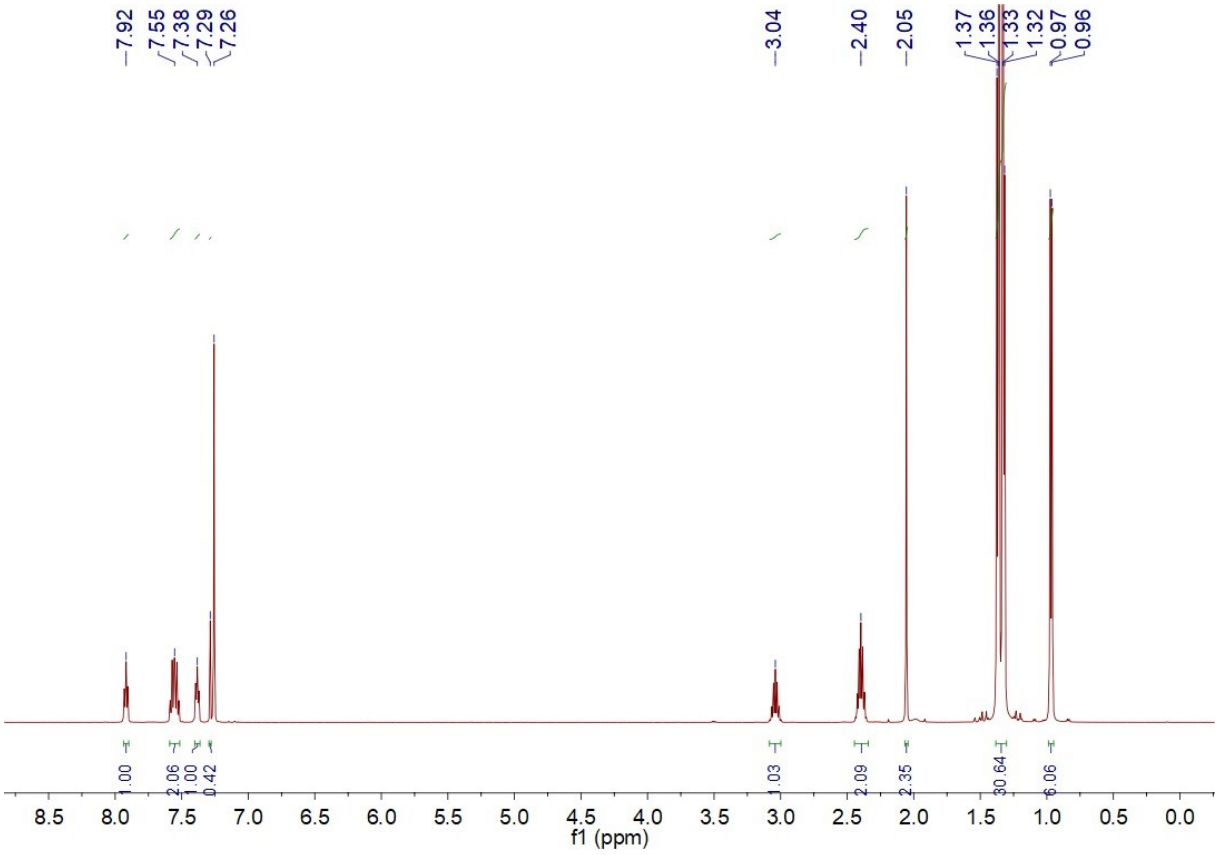

Figure S8. ^{1}H NMR spectrum of **3** ($CDCl_3$)

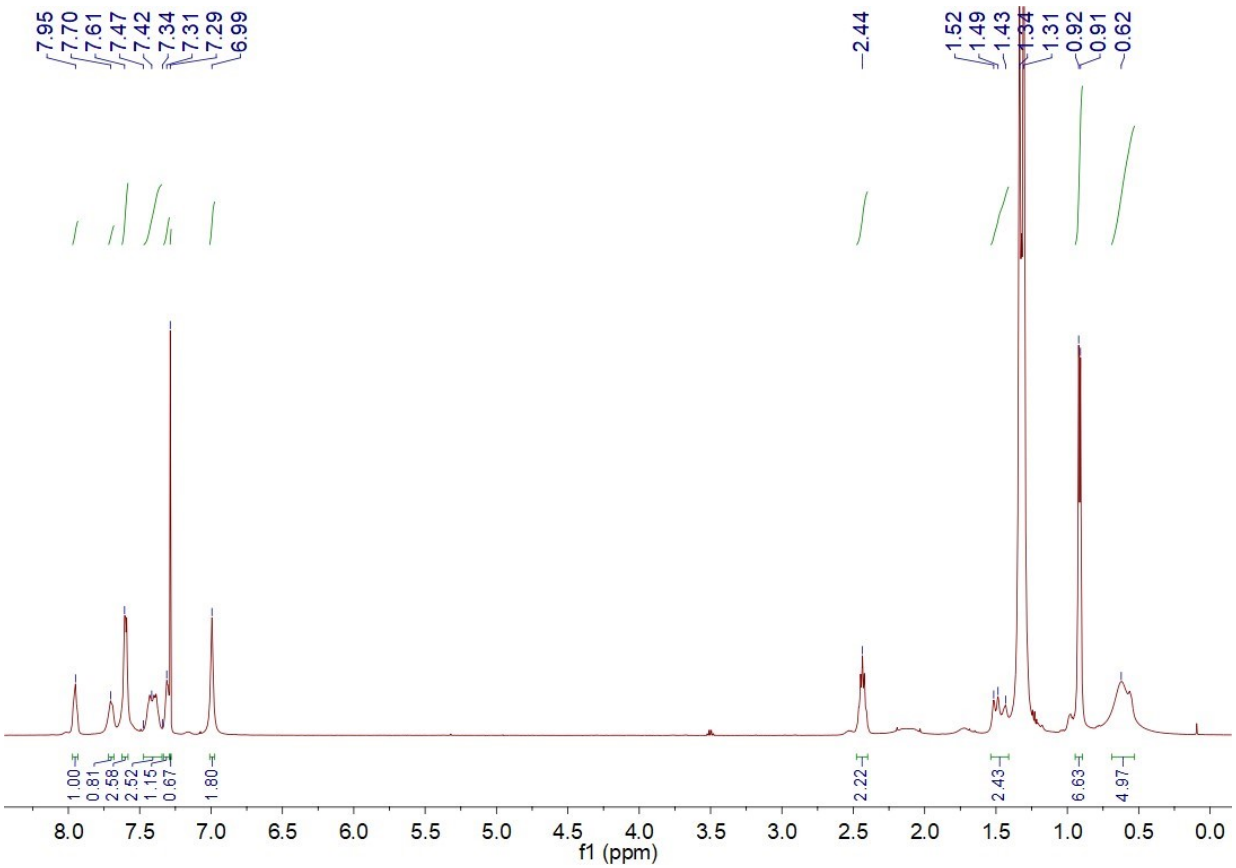

Figure S9. ^{1}H NMR spectrum of **4** (in $CDCl_3$)

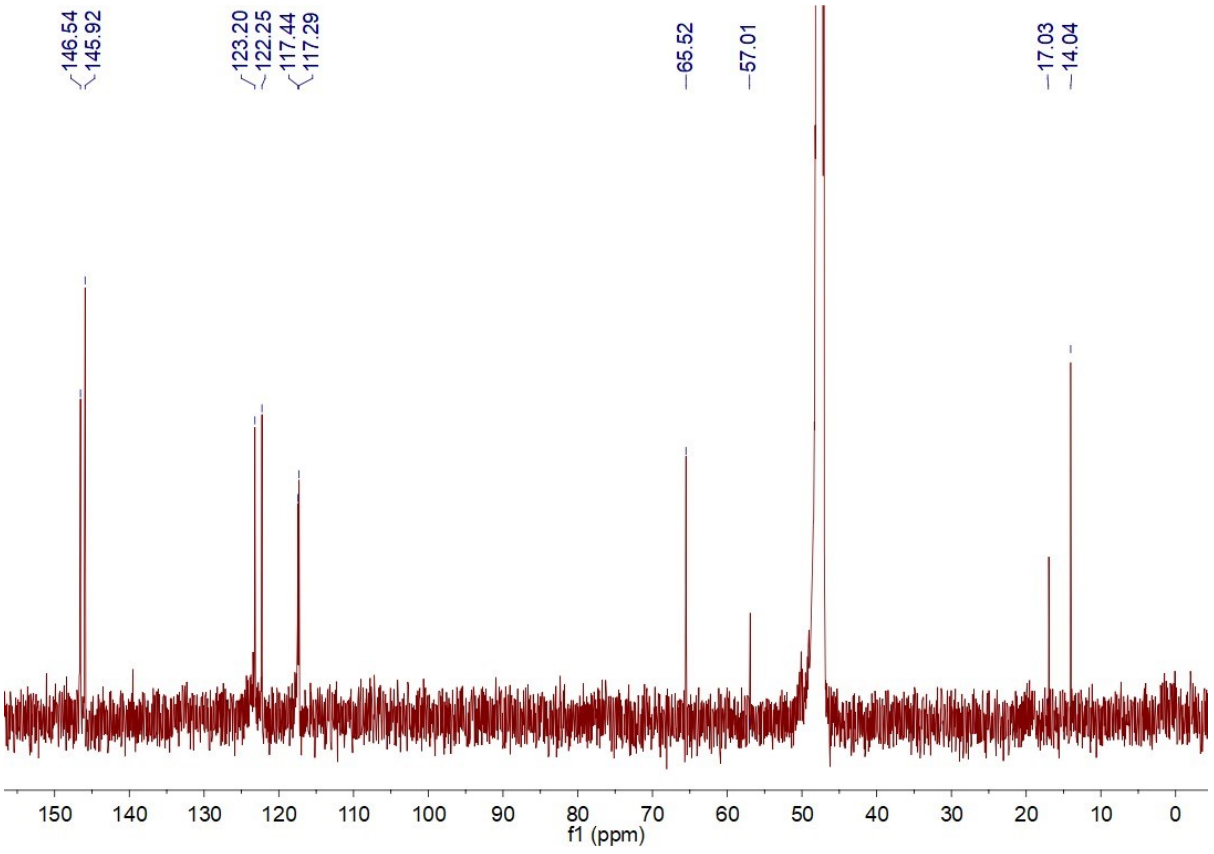

Figure S10. $^{13}C\{H\}$ NMR spectrum of **2** (in CD_3OD)

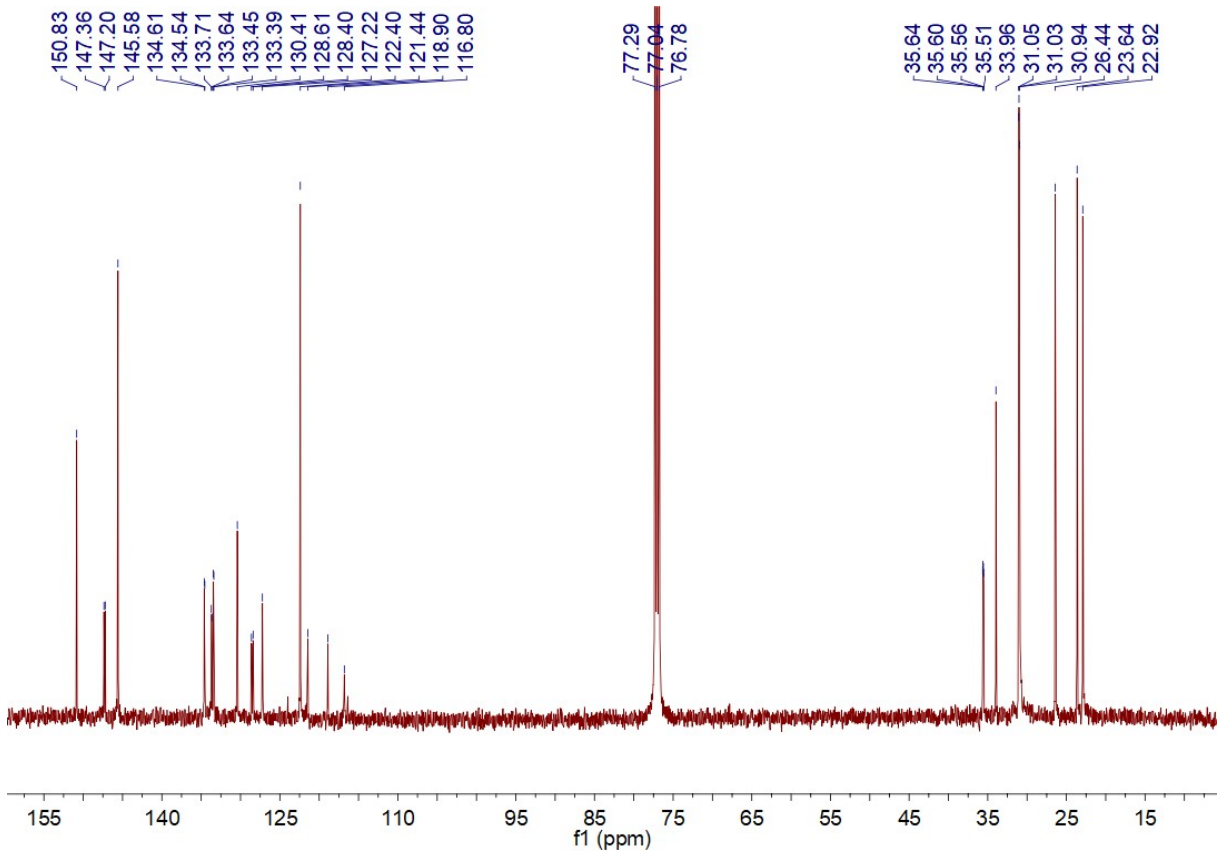

Figure S11. $^{13}C\{H\}$ NMR spectrum of **3** (in $CDCl_3$)

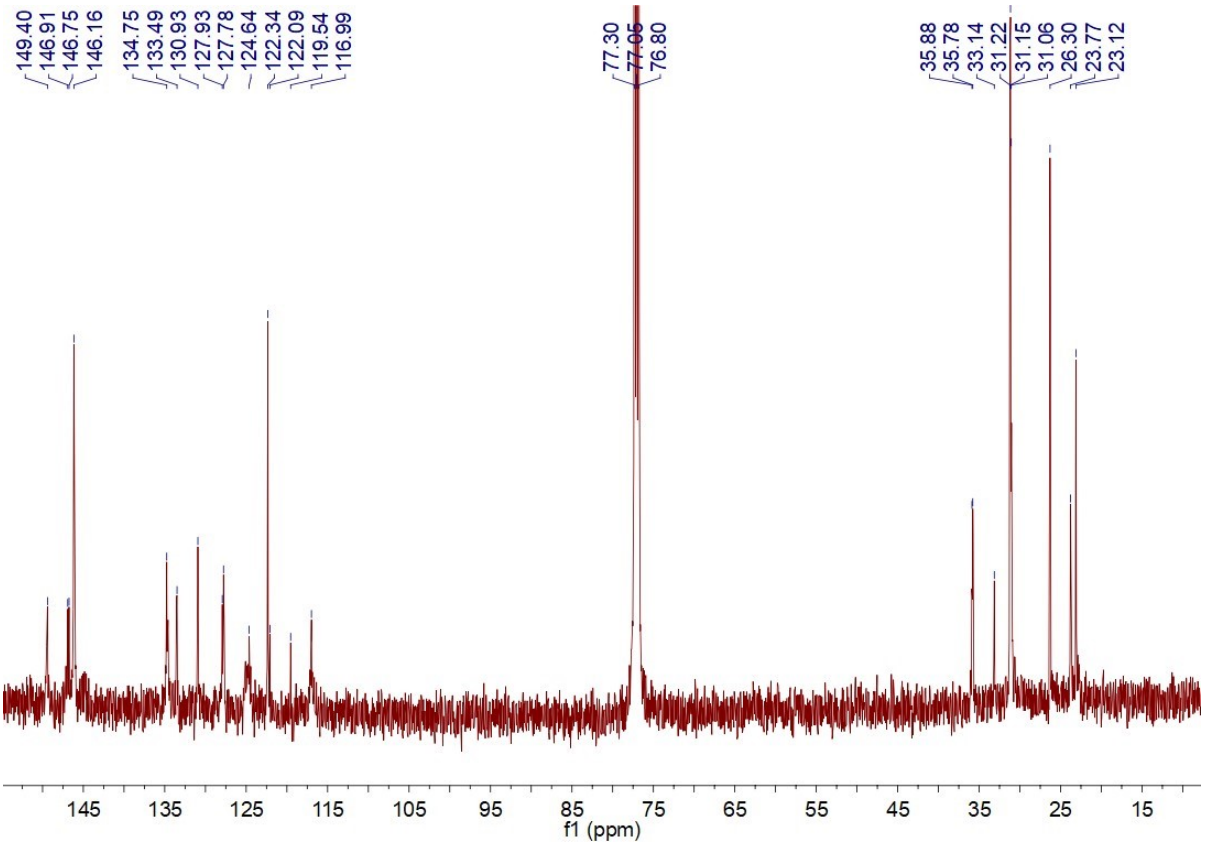

Figure S12. $^{13}C\{H\}$ NMR spectrum of **4** (in $CDCl_3$)

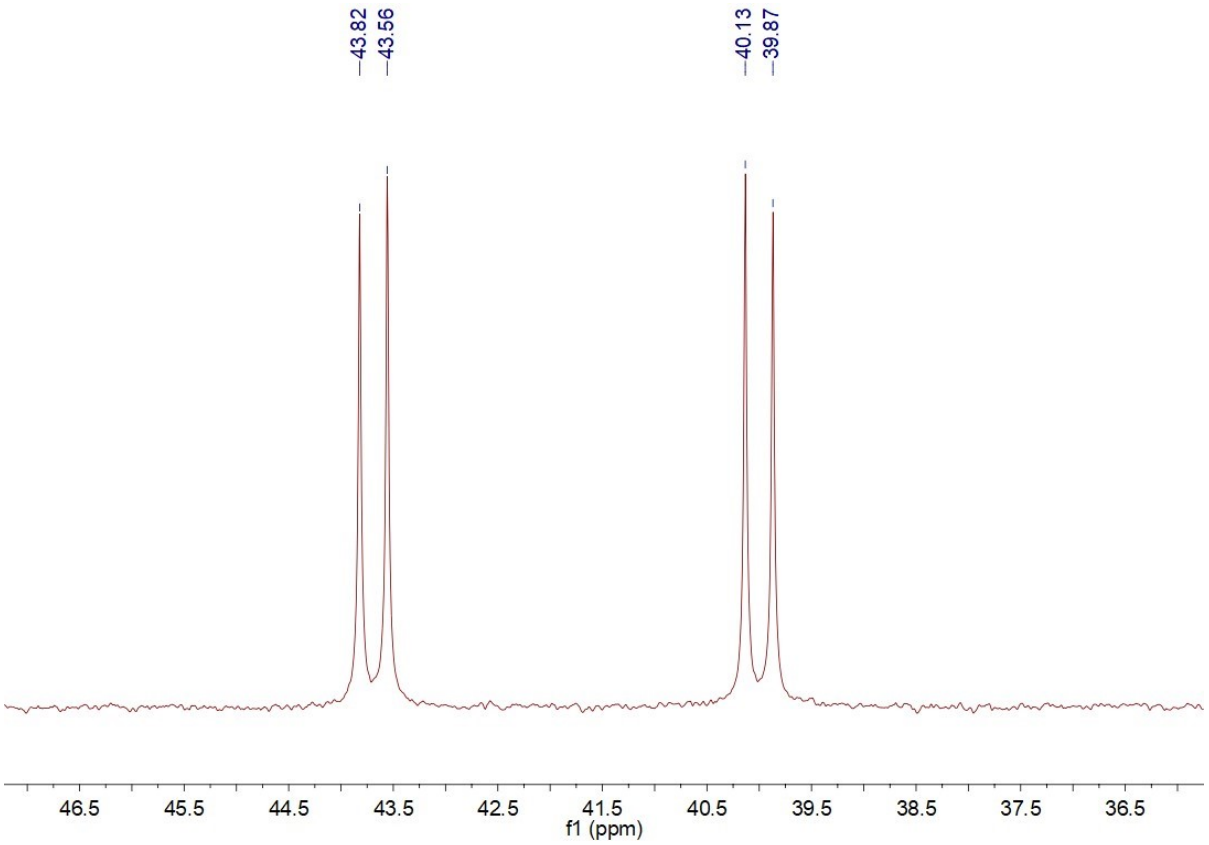

Figure S13. ^{31}P NMR spectrum of **3** (in $CDCl_3$).

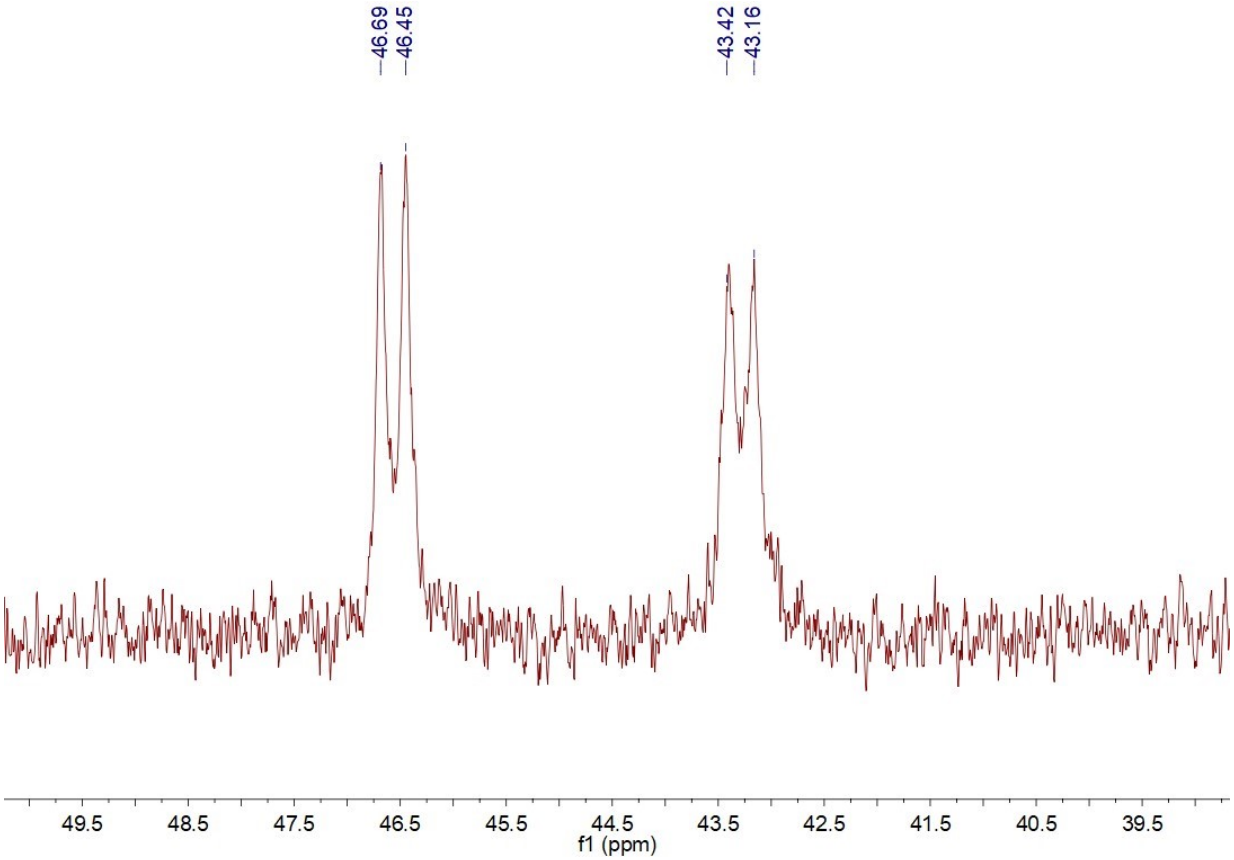

Figure S14. ^{31}P NMR spectrum of **4** (in CD_2Cl_2).

IR Spectra

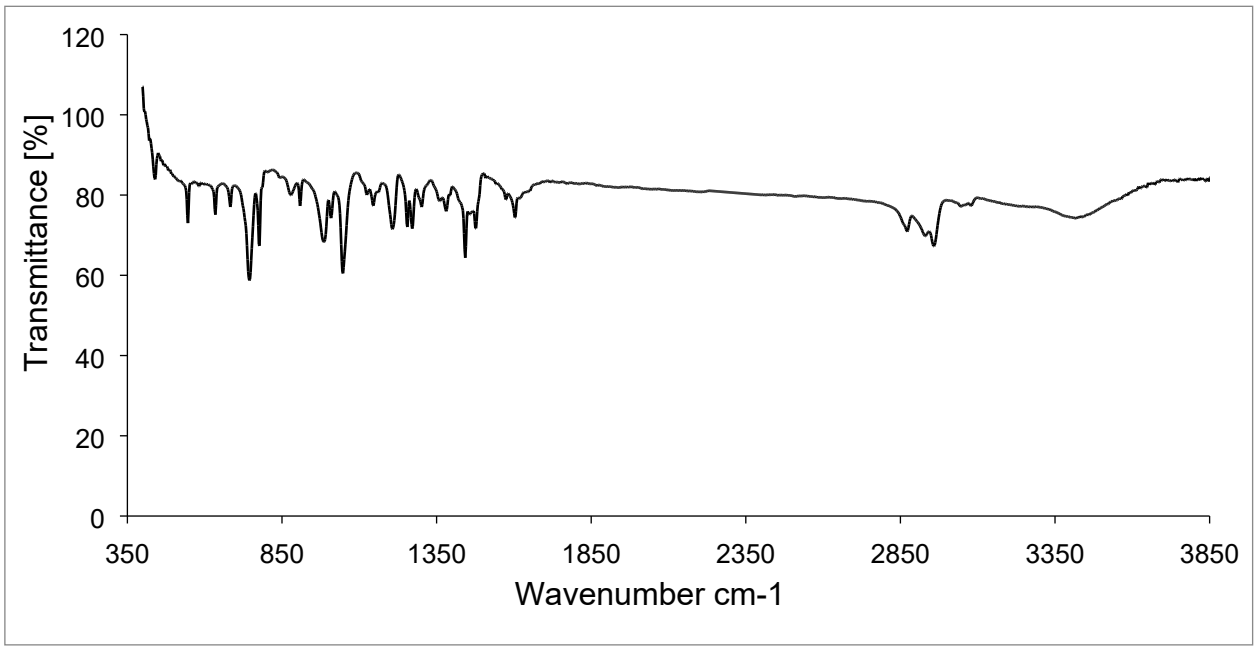

Figure S15. IR Spectrum of **1**.

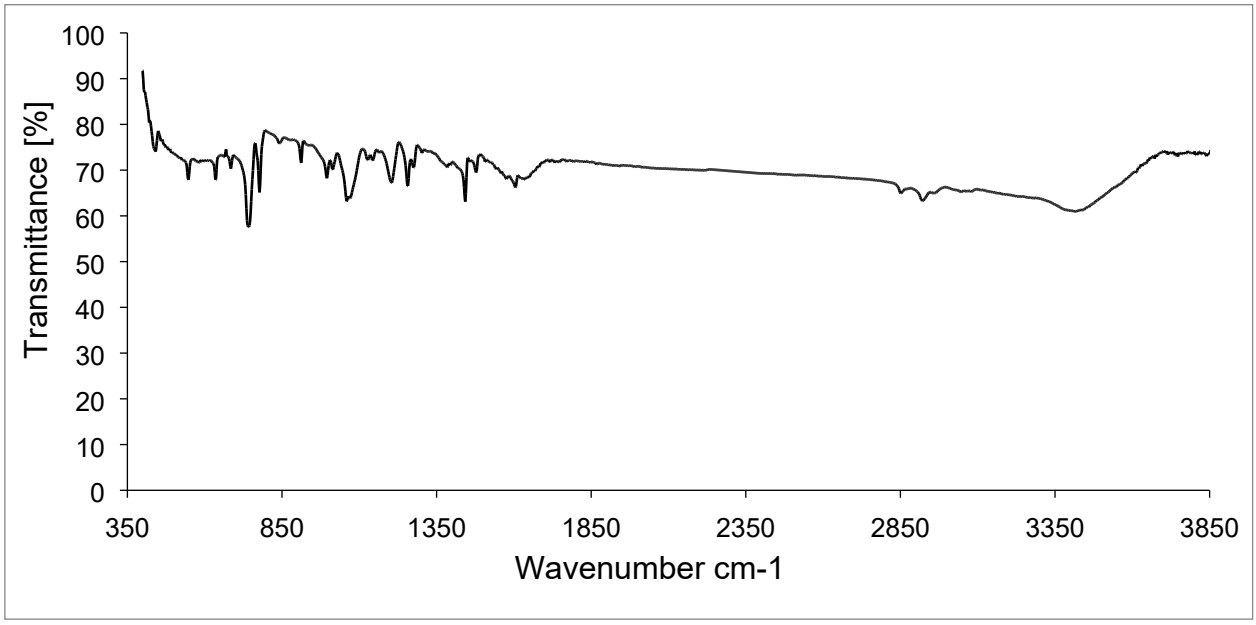

Figure S16. IR Spectrum of **2**.

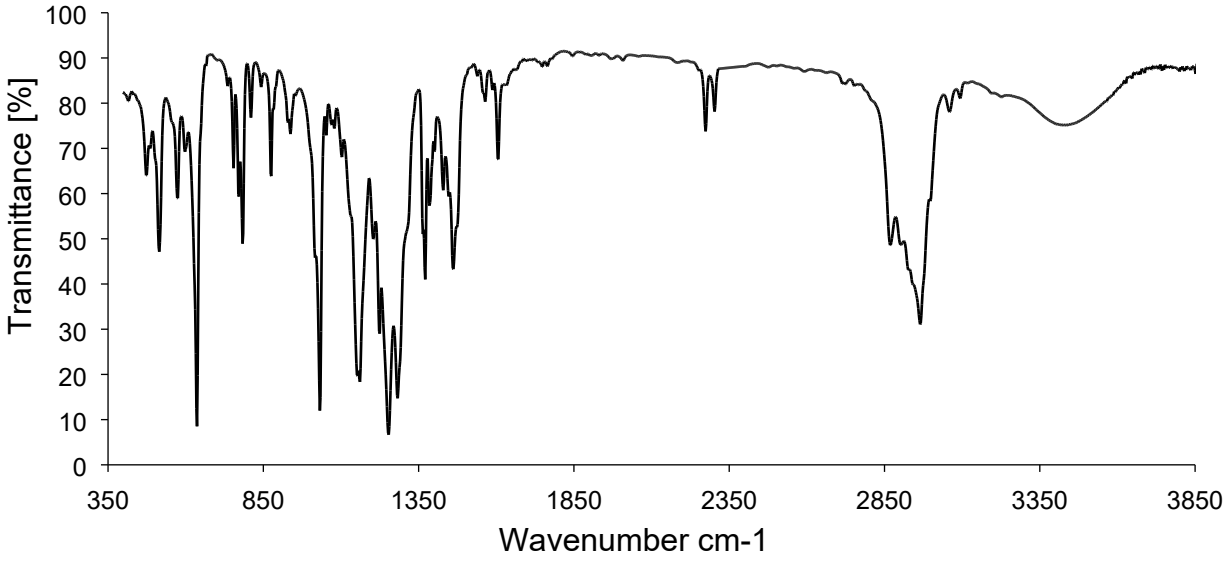

Figure S17. IR Spectrum of **3**.

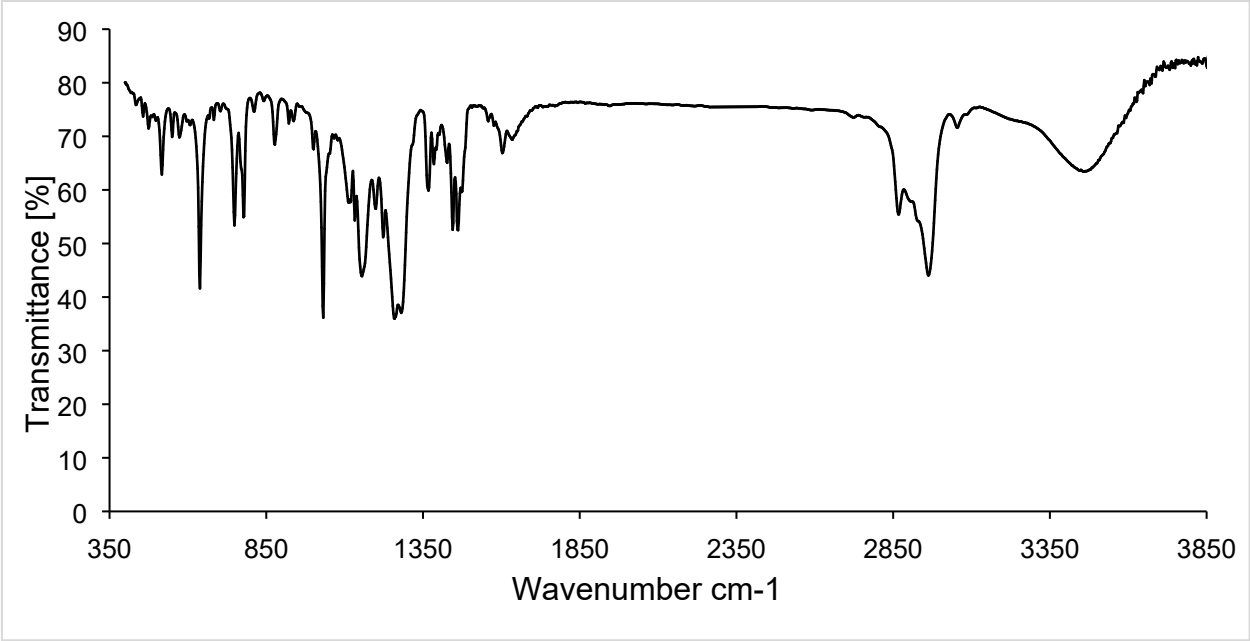

Figure S18. IR Spectrum of **4**.

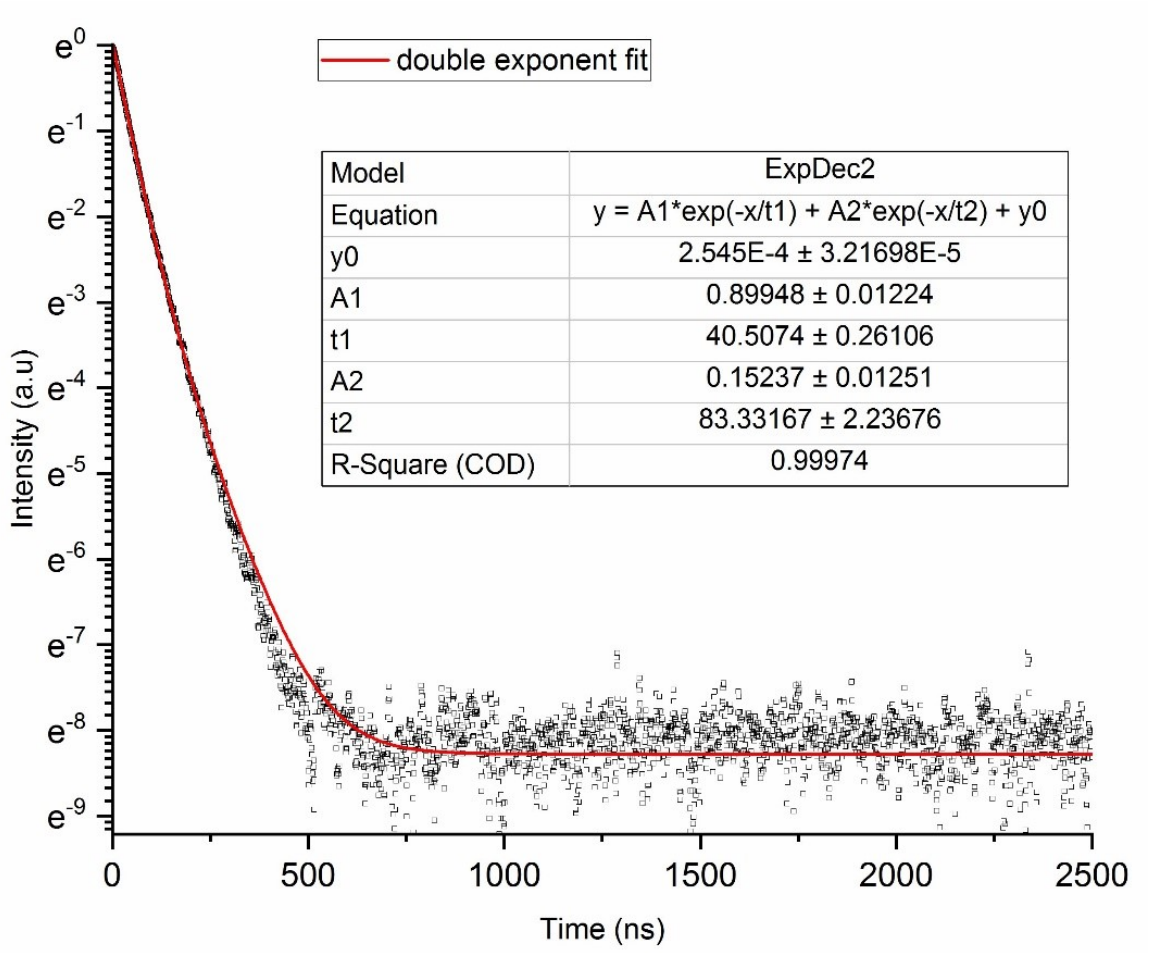

Fig. S19. Luminescence decay kinetics of **2** at room temperature.

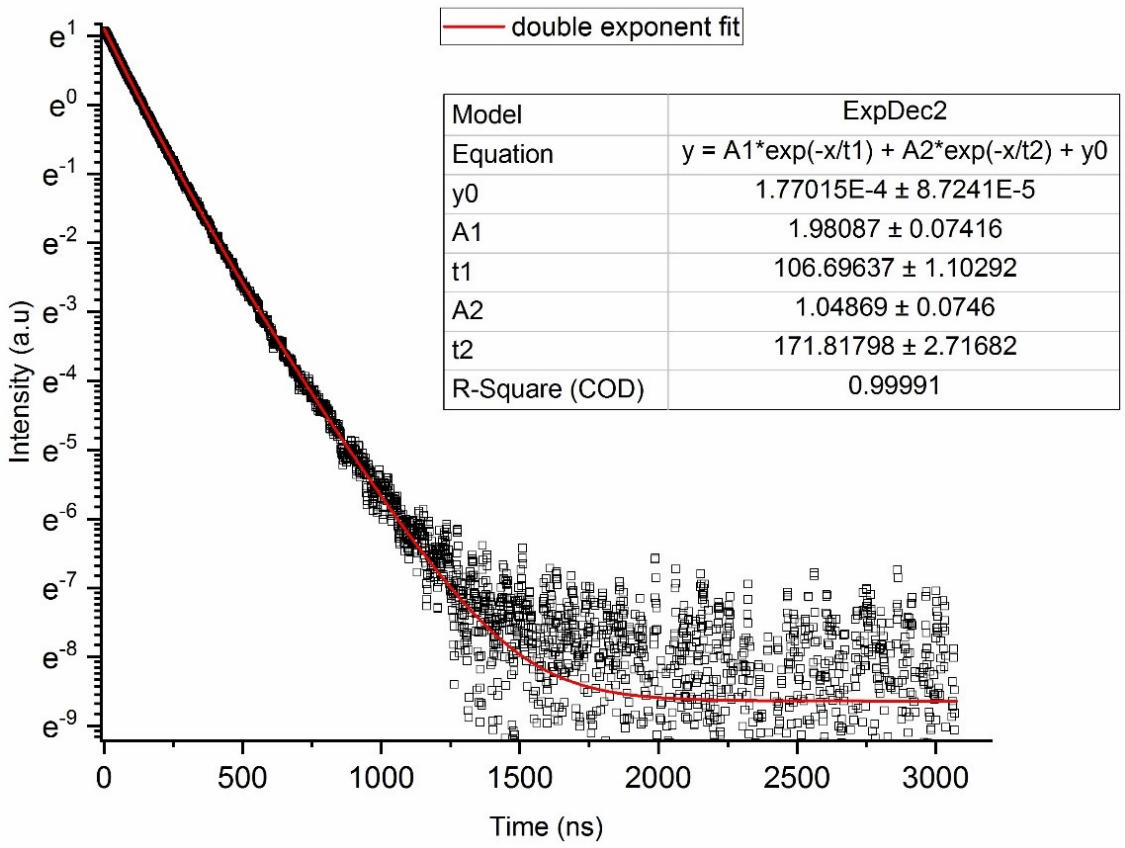

Fig. S20. Luminescence decay kinetics of **2** at 80K

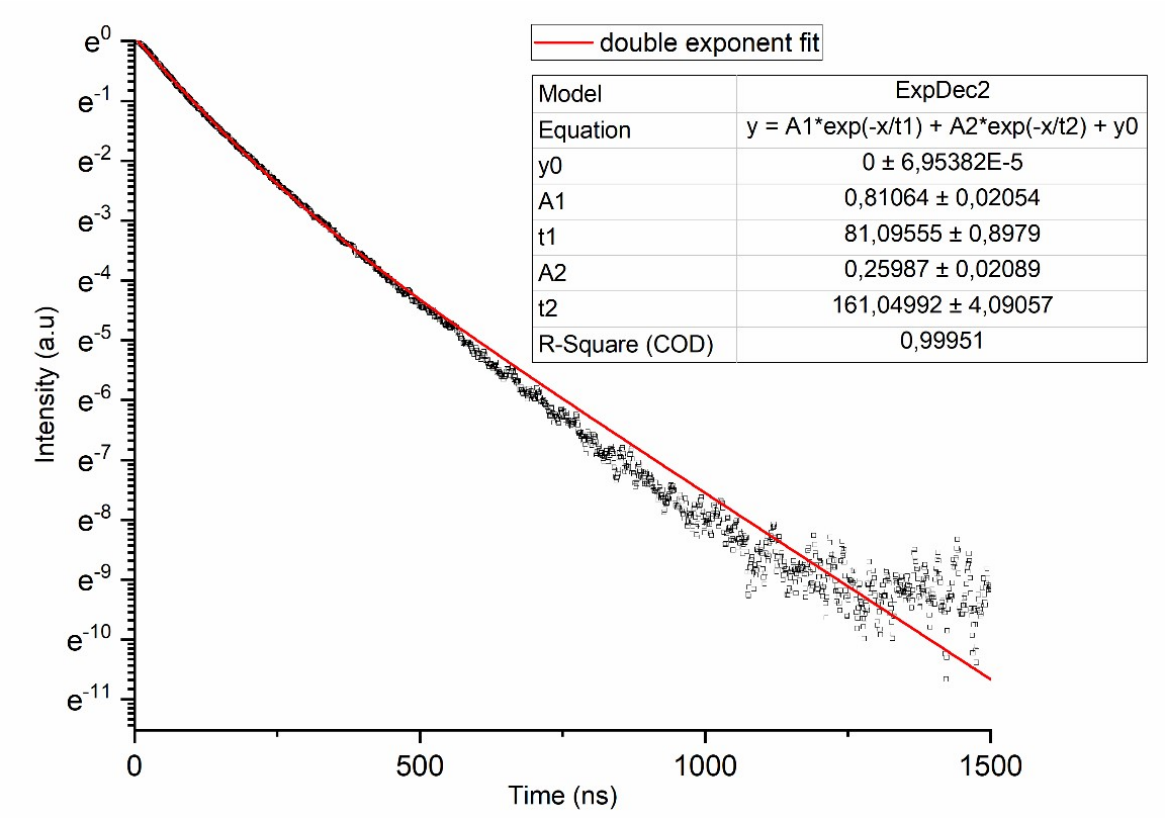

Fig. 21. Luminescence decay kinetics of **4** at RT

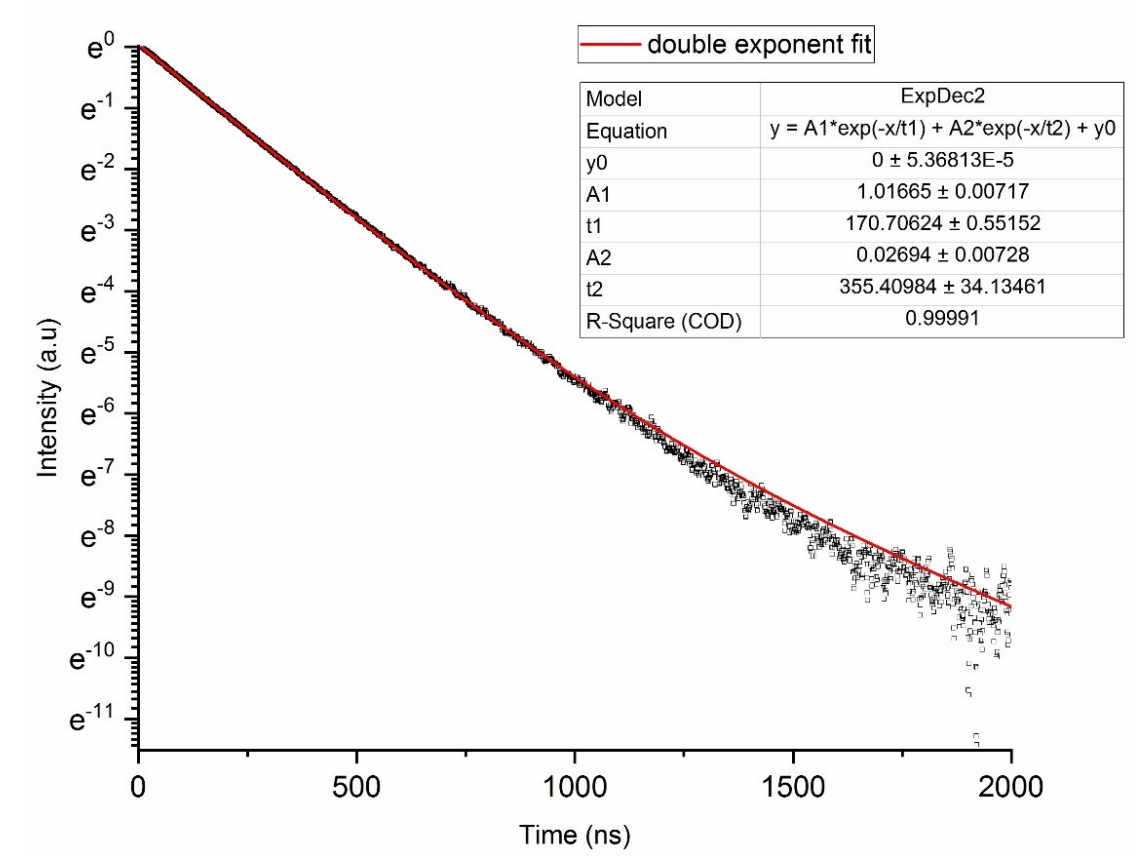

Fig. 22. Luminescence decay kinetics of **4** at 80K

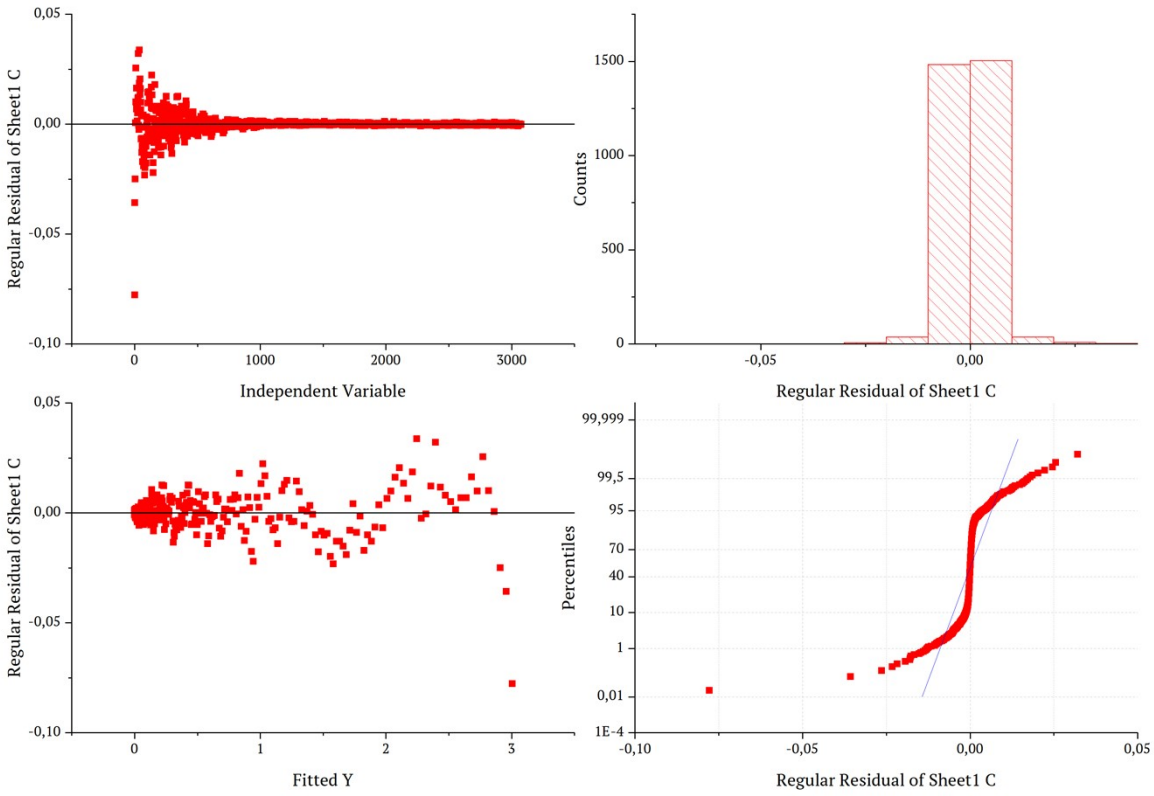

Fig. S23. Approximation of decay kinetics graph for the complex **2** at RT.

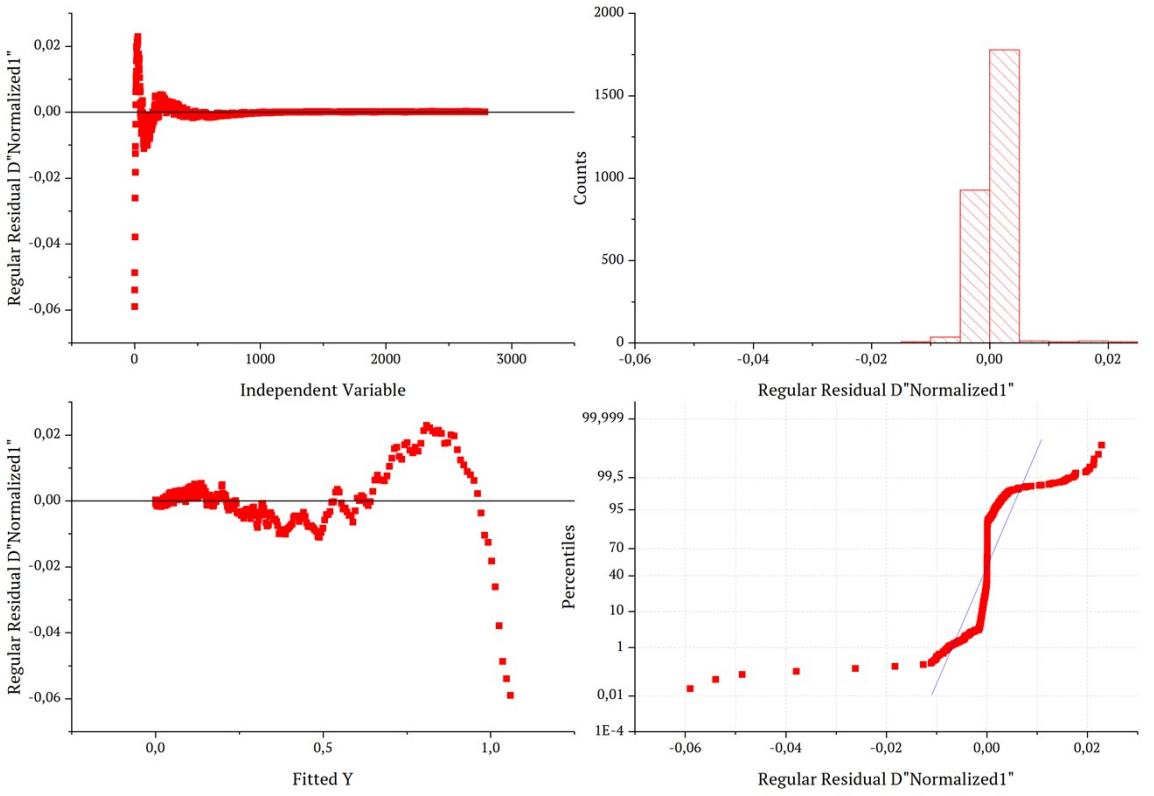

Fig. S24. Approximation of decay kinetics graph for the complex **4** at RT.

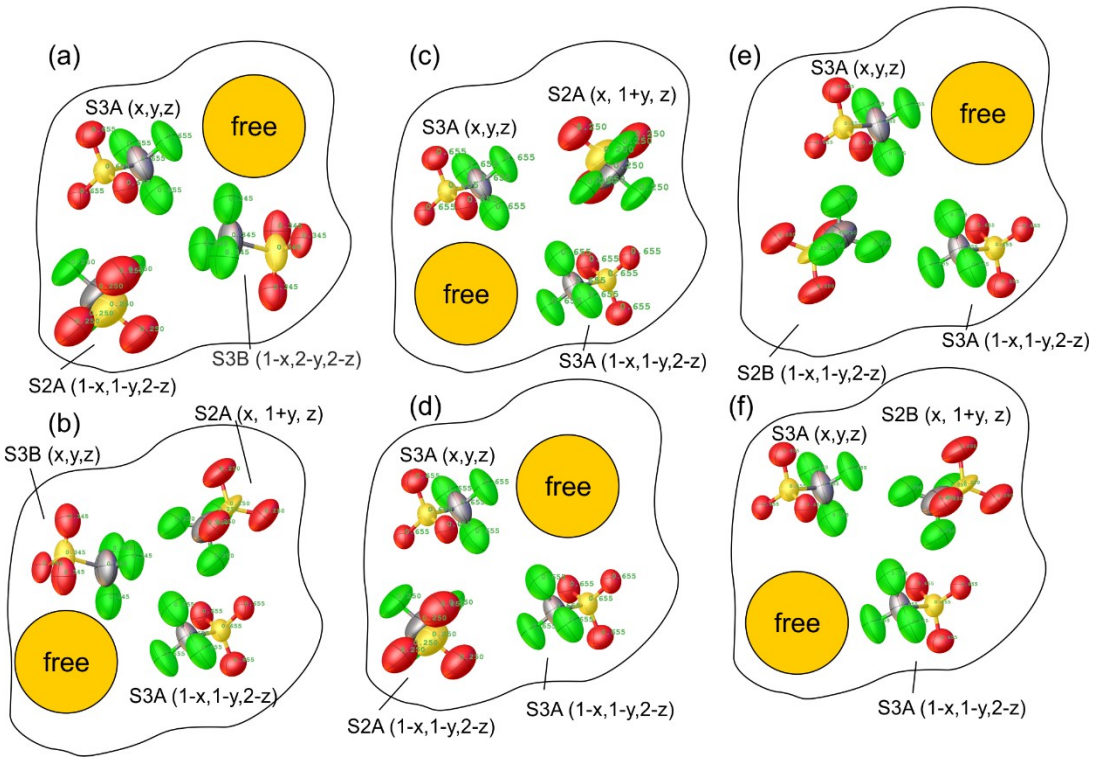

Fig. S25. Disorder model of triflate anions within the cavity in the structure of **4b**.

Six geometrically feasible combinations of occupied triflate positions are listed with symmetry codes. Schematically outlined cavity comprises three triflates (1.5 triflates for crystallographically independent half of the cavity). S2A/S2B triflate is disordered over 4 positions and has an occupancy of 0.25 each, ensuring that only one of these four positions is occupied at any given cavity. S3A/S3B triflate is disordered over 4 positions, with a total combined occupancy of 2 across the two symmetry-equivalent positions. Position not occupied by triflate is marked as "free". Possible variants are: a) S3A (x, y, z), S3B (1-x, 2-y, 2-z), and S2A (1-x, 1-y, 2-z); b) S3B (x, y, z), S3A (1-x, 2-y, 2-z), and S2A (x, 1+y, z); c-f) S3A (x, y, z), S3A (1-x, 2-y, 2-z), and either S2A (1-x, 1-y, 2-z), S2A (x, 1+y, z), S2B (x, 1+y, z), or S2B (1-x, 1-y, 2-z). NOT feasible variants are: S3B, S3B(1-x, 2-y, 2-z), any of S2A or S2B; S3A (x, y, z), S3B (1-x, 2-y, 2-z), and either S2B (x, 1+y, z), S2B (1-x, 2-y, 2-z), or S2A (x, 1+y, z); S3A (1-x, 2-y, 2-z), S3B (x, y, z), and either S2A (1-x, 2-y, 2-z), S2B (1-x, 2-y, 2-z), or S2B (x, 1+y, z). The cavity volume is approximately 600 Å^3, which is sufficient to accommodate three triflate anions. The van der Waals volume of a triflate anion is ca. 80 Å^3, while the effective volume required in a crystalline environment is typically 160–170 Å^3 per triflate. Three triflates thus require approximately 480–510 Å^3; the remaining "free" position could be accommodated by disordered solvent molecules.

Reference

1. M. A. Mikhailov, K. A. Brylev, P. A. Abramov, E. Sakuda, S. Akagi, A. Ito, N. Kitamura and M. N. Sokolov, *Inorg. Chem.*, 2016, **55**, 8437–8445.
2. G. M. Whitesides and F. D. Gutowski, *J. Org. Chem.*, 1976, **41**, 2882–2885.
3. V. Logvinenko, O. Polunina, Yu. Mikhailov, K. Mikhailov and B. Bokhonov, *J. Therm. Anal. Calorim.*, 2007, **90**, 813–816.
4. G. M. Sheldrick, SHELXT– Integrated space-group and crystal-structure determination*, Acta Crystallogr. A Found Adv.* 2015, **71**, 3–8.
5. G. M. Sheldrick, Crystal structure refinement with SHELXL*, Acta Crystallogr. C Struct. Chem.* 2015, **71**, 3–8.
6. O. V. Dolomanov, L. J. Bourhis, R. J. Gildea, J. A. K. Howard, H. Puschmann, *OLEX2: a complete structure solution, refinement and analysis program, J. Appl. Crystallogr.* 2009, **42**, 339–341.
7. a) A. V. Alexeev and S. A. Gromilov, Quantitative phase analysis on a single crystal X-ray diffractometer equipped with a two-dimensional flat detector, *J. Struct. Chem.*, 2010, **51**, 156–165.
8. A. V. Alexeev and S. A. Gromilov, X-Ray Diffraction Study of Micro Amounts of Polycrystalline Samples, *J. Struct. Chem.*, 2010, **51**, 744–757.
9. C. Prescher and V. B. Prakapenka, DIOPTAS: a program for reduction of two-dimensional X-ray diffraction data and data exploration, *High Press. Res.*, 2015, **35**, 223–230.
10. K. Kirakci, P. Kubát, M. Dušek, K. Fejfarová, V. Šícha, J. Mosinger and K. Lang, *Eur. J. Inorg. Chem.*, 2012, 3107–3111.
11. S. Akagi, S. Fujii, T. Horiguchi and N. Kitamura, *J. Clust. Sci.*, 2016, **28**, 757–772.
12. K. Kirakci, K. Fejfarová, M. Kučeráková and K. Lang, *Eur. J. Inorg. Chem.*, 2014, 2331–2336.
13. K. Kirakci, P. Kubát, K. Fejfarová, J. Martinčík, M. Nikl and K. Lang, *Inorg. Chem.*, 2015, **55**, 803–809.
14. K. Kirakci, J. Zelenka, I. Křížová, T. Ruml and K. Lang, *Inorg. Chem.*, 2020, **59**, 9287–9293.
15. D. V. Evtushok, A. R. Melnikov, N. A. Vorotnikova, Y. A. Vorotnikov, A. A. Ryadun, N. V. Kuratieva, K. V. Kozyr, N. R. Obedinskaya, E. I. Kretov, I. N. Novozhilov, Y. V. Mironov, D. V. Stass, O. A. Efremova and M. A. Shestopalov, *Dalton Trans*., 2017, **46**, 11738–11747.
16. K. Kirakci, V. Šícha, J. Holub, P. Kubát and K. Lang, *Inorg. Chem.*, 2014, **53**, 13012–13018.
17. O. A. Efremova, Y. A. Vorotnikov, K. A. Brylev, N. A. Vorotnikova, I. N. Novozhilov, N. V. Kuratieva, M. V. Edeleva, D. M. Benoit, N. Kitamura, Y. V. Mironov, M. A. Shestopalov and A. J. Sutherland, *Dalton Trans.*, 2016, **45**, 15427–15435.
18. M. Prévôt, M. Amela-Cortes, S. K. Manna, R. Lefort, S. Cordier, H. Folliot, L. Dupont and Y. Molard, *Adv. Funct. Mater.*, 2015, **25**, 4966–4975.
19. K. Kirakci, T. N. Pozmogova, A. Y. Protasevich, G. D. Vavilov, D. V. Stass, M. A. Shestopalov and K. Lang, *Biomater. Sci.*, 2021, **9**, 2893–2902.